Journal of Robotics and Control (JRC)
Volume 4, Issue 2, March 2023
ISSN: 2715-5072, DOI: 10.18196/jrc.v4i2.17433

A New Self-Tuning Nonlinear PID Motion Control for One-Axis Servomechanism with Uncertainty Consideration

Mohamed A. Shamseldin [1]*, M. A. Abdelghany [2]
[1] Faculty of Engineering and Technology, Future University in Egypt, Cairo, Egypt
[2] Faculty of Engineering, 6 October University, Giza, Egypt
Email: [1] mohamed.abelbbar@fue.edu.eg, [2] M.a.abdelghany.eng@o6u.edu.eg
* Correspondence Author

***Abstract*— this paper introduces a new study for one-axis servomechanism with consideration the parameter variation and system uncertainty. Also, a new approach for high-performance self-tuning nonlinear PID control was developed to track a preselected profile with high accuracy. Moreover, a comparison study between the proposed control technique and the well-known controllers (PID and Nonlinear PID). The optimal control parameters were determined based on the COVID-19 optimization technique. The parameters of the servomechanism system changed randomly at a preselected range through the online simulation. The change of these parameters acts as the nonlinearity resources (friction, backlash, environmental effects) and system uncertainty. A comparative study between the linear and nonlinear models had been accomplished and investigated. The results show that the proposed controller can track several operating points with high accuracy, low rise time, and small overshoot.**

Keywords—Servomechanism; PID control; Nonlinear PID control; COVID-19; Uncertainty

I. INTRODUCTION

The main component of the majority of CNC machines is the one-stage servomechanism system [1], [2]. For these machines to manufacture goods of a high caliber, exact motion control is required [3], [4]. Additionally, numerous high-speed and high-accuracy position applications have been rapidly made to support sophisticated automatic industrial processes [5], [4].

The friction and backlash models' parameters are typically unknown for servomechanism systems, which causes system uncertainty [6], [7]. High steady-state error is caused by friction, while unwanted vibration is caused by blowback [8], [9]. There hasn't been a concrete model developed yet to explain accurately the friction issue in servomechanism systems[10], [11].

As a result, the control task for this procedure is quite difficult. For single-axis controllers, there are numerous design strategies available, including traditional PID control, self-tuning PID control, fuzzy PID control, adaptive control, and sliding mode control [12]-[15].

The benefit of the sliding mode technique is that it offers good tracking performance throughout a range of position command operating points [16], [11]. On the other side, chattering phenomena can make it difficult to increase control accuracy and, in rare situations, it can lead to system instability [17]-[19]. The fuzzy logic system is an effective method for handling complex systems' nonlinearity and uncertainty issues. But, it needs big memory data and high processing speed [20]-[24]. Also, the neural network needs a high training time and big data storage. So, most industrial applications use the conventional PID control or Nonlinear PID control which achieves a satisfactory response for traditional applications (pick and place tasks or low accuracy motion) [25]-[28].

It is well known that Model Reference Adaptive Control (MRAC) is a very effective adaptive control that compels the entire system to behave by a predetermined model reference. Depending on the designer's viewpoint, the chosen model reference may be a first-order or second-order system. Although MRAC performs quickly, some systems may not like the high overshoot it experiences [29]-[33].

The nonlinear PID controller consists of six parameters which are classified into two parts, the first part is the traditional PID parameters while the second part is the fixed three parameters integrated into the nonlinear function [34]-[38]. This type of controller has a satisfying behavior with several nonlinear systems but it has a poor performance when there are uncertainty and parameter variations [39], [40].

This paper seeks to develop a new self-tuning for these six parameters at the same time online using an adaptive mechanism based on a preselected model reference. The proposed control technique treats the nonlinearity resources such as friction and backlash. Also, it can deal with the uncertainty problem without using a complex model for friction and backlash. A friction Compensation Method for Servomechanism was presented in [41]. Analysis of limit cycle mechanism for two-mass system with backlash nonlinearity was demonstrated in [42]. Sinusoidal servo compensator implementations with real-time requirements and applications was presented in [43]. Dynamic analysis of an XY positioning table was illustrated in [44]. Evaluation on tracking performance of PID, gain scheduling and classical cascade p/pi controller on XY table balls crew drive system was displayed in [45].

The paper is prepared as following, firstly, the system modeling is presented. Secondly, the proposed control

techniques are demonstrated. Thirdly, the results are illustrated. Finally, the conclusion is discussed.

II. System Modeling

This section demonstrates the single-axis model in two forms. The first model presents a linear behavior without parameter variations and uncertainty. The second model was developed to simulate the actual uncertainty and nonlinearity. This paper can define uncertainty as the random change in system parameters. Fig. 1 shows the general structure of the single-axis servomechanism.

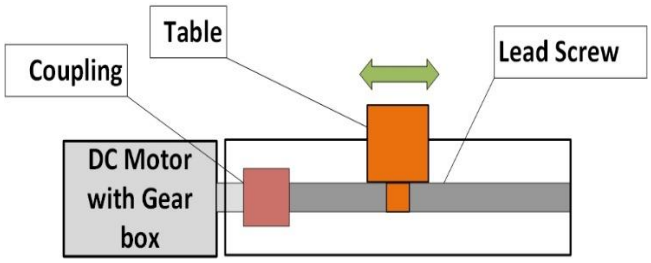

Fig. 1. A simple structure of the battery electric vehicle

The DC motor model can describe from equation (1) to equation (3) where X_a is the armature voltage, W_a is the armature resistance, I_a is armature current, D_a is the inductance of motor windings, K_b is the back emf constant, ρ is the rotor speed, ϑ_m is the motor torque, K_t is the torque constant, ε_e is the total equivalent moment of inertia as seen by the motor, B is the viscous damping coefficient and ϑ_s is the total static torque reflected in the lead screw shaft.

$$X_a = W_a I_a + D_a \frac{di_a}{dt} + K_b \rho \tag{1}$$

$$\vartheta_m = K_t \, i_a \tag{2}$$

$$\vartheta_m = \varepsilon_e \dot{\rho} + B\rho + \vartheta_s \tag{3}$$

There are three sources for the total static torque reflected in the lead screw shaft (ϑ_s) as in equation (4) where ϑ_{gf} is the static torque contributed by the friction in the guideways, ϑ_{lf} is the torque lost in bearings due to friction, ϑ_f is the torque required to overcome the feed forces.

$$\vartheta_s = \vartheta_{gf} + \vartheta_{bf} + \vartheta_f \tag{4}$$

In the case of a gear between the motor shaft and the lead screw shaft the ϑ_s will be determined as equation (5) where ϵ_g is the gear reduction.

$$\vartheta_{sr} = \frac{\vartheta_s}{\epsilon_g} \tag{5}$$

Equation (6) illustrates the static torque due to guideways friction where $\emptyset$ is pitch of lead screw, μ_{gf} is the friction coefficient in guides, m_t is the table mass, m_w is the maximum mass for the workpiece and F_z is the maximum vertical force.

$$\vartheta_{gf} = \frac{\emptyset}{2\pi} \, \mu_{gf} (\, (m_t + m_w) g + F_z) \tag{6}$$

Equation (7) demonstrates the lost static torque due to bearing friction where μ_b is the friction coefficient of bearings, d_p is the leadscrew diameter, F_f is the maximum feeding force and F_p is preload force in the thrust bearings.

$$\vartheta_{bf} = \frac{d_p}{2} \, \mu_b (F_f + F_p) \tag{7}$$

The required torque to overcome feed forces can be calculated as (8).

$$\vartheta_f = \frac{\emptyset}{2\pi} F_f \tag{8}$$

The total equivalent moment of inertia as seen by the motor (ε_e) depends on ε_{tw} the moment of inertia of table and workpiece reflected on the lead screw shaft, ε_L is the lead screw inertia and ε_m motor shaft inertia can be calculated as (9).

$$\varepsilon_e = \frac{\varepsilon_{tw} + \varepsilon_L}{\epsilon_g^2} + \varepsilon_m \tag{9}$$

The moment of inertia of table and workpiece can be determined based on mass table (m_t) and maximum mass of workpiece (m_w) as shown in (10).

$$\varepsilon_{tw} = (m_t + m_w)(\frac{\emptyset}{2\pi}) \tag{10}$$

The lead screw moment inertia is determined using lead screw mass as equation (11).

$$\varepsilon_L = \frac{1}{2} \, m_L (\frac{d_p}{2})^2 \tag{11}$$

Equation (1) will be reorganized to obtain as in (12).

$$i_a = \frac{X_a - K_b \rho}{D_a s + W_a} \tag{12}$$

Also, equation (3) will be reformed to result as in (13).

$$\rho = \frac{\vartheta_m - \vartheta_s}{\varepsilon_e s + W_a} \tag{13}$$

Equations (12) and (13) are used to build the DC motor model incorporated with servomechanism system, so obtained model as (14).

$$\rho(s) = G_1(s) X_a(s) + \, G_2(s) \, \vartheta_s(s) \tag{14}$$

To find the transfer function between ω and v_a assumes $T_s = 0$, as shown in the equation (15).

$$G_1(s) = \frac{\rho(s)}{X_a(s)} = \frac{K_t}{D_a \varepsilon_e s^2 + \varepsilon_e W_a s + K_t K_b} \tag{15}$$

To obtain the transfer function between ρ and ϑ_s assumes $X_a = 0$ will result the following transfer function in as equation (16).

$$G_2(s) = \frac{\rho(s)}{\vartheta_s(s)} = \frac{-(D_a s + W_a)}{D_a\ \varepsilon_e s^2 + (D_a B + \varepsilon_e R_a)s + (W_a B - K_t K_b)} \quad (16)$$

The actual position table can be calculated using equation (17).

$$\beta_{act}(s) = \frac{\emptyset}{2\pi}\frac{1}{s}\rho(s) \quad (17)$$

To simulate the uncertainty and nonlinearity of the servomechanism, the system parameters will change randomly online. For example, to imitate the backlash behavior the ϵ_g, ε_e and $\emptyset$ will be changed continuously online. Also, to capture the friction behavior the μ_{gf}, μ_b and B will be fluctuated in a preselected range randomly. Moreover, the motor uncertainty will be executed by change the W_a and D_a randomly.

The following Table 1 shows the system parameters values and the borders of change.

TABLE I. FIXED PARAMETERS OF THE SERVOMECHANISM SYSTEM.

No.	Parameter	Unit	Definition	Borders of change
1	$\emptyset$=0.00508	m/rev	Pitch of feed screw	0.005~ 0.0051
2	ϵ_g=1	------	Gear reduction ratio	0.8~ 1.2
3	Da=0.5	ohm	Motor winding resistance	0.45~ 0.55
4	ε_m=2.373×10^{-3}	Kg.m^2	Motor shaft inertia	2.3×10-3~ 2.4×10-3
5	B = 0	Nm/(rad/sec)	Viscous damping ratio	0.00001~ 0.00002
6	μ_{gf} = 0.1	-----	Friction coefficient in guides	0.95~ 0.15
7	μ_b= 0.005	------	Bearings Friction coefficient	0.0045~ 0.0055

The following Table 2 demonstrates the fixed parameters of servomechanism system.

TABLE II. VARIABLE PARAMETERS OF THE SERVOMECHANISM SYSTEM.

No.	Parameter	Unit	Definition
1	mt=180	kg	table mass
2	mw=200	kg	max mass workpiece
3	mL=8.15	kg	leadscrew mass
4	dp=0.0445	m	Feed screw diameter
5	fz=2000	N	max vertical force
6	Ff=8000;	N	max feeding force
7	Fp=5000	N	preload force in thrust bearing
8	f=0.170	N	rapid traverse velocity m/s
9	tr=0.1	sec	servo rise time sec
10	X_a=220	V	Motor rated voltage

Fig. 2 shows the motor voltage input which changed as form a sin wave to investigate the output stage position of servomechanism. It can be noted that the input voltage is applied on the linear and nonlinear model as demonstrated in Fig. 3.

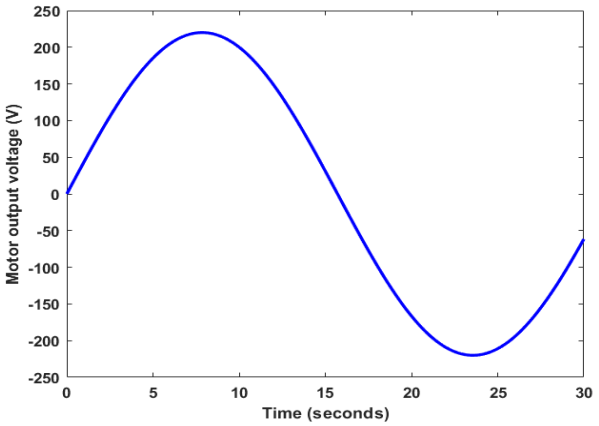

Fig. 2. The input voltage for DC motor.

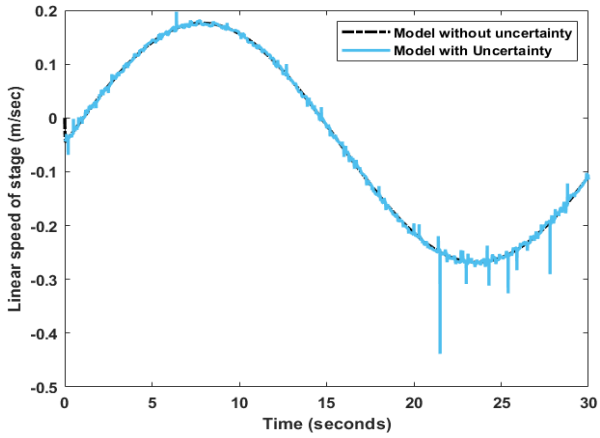

Fig. 3. The corresponding output position of servomechanism.

III. COVID-19 OPTIMIZATION

There are many methods to define the parameters of the PID controller such as try and error and Ziegler-Nichols methods but most of these methods are rough roads. This study introduces a new effective optimization technique which is the COVID-19 optimization algorithm to find the optimal parameters of the proposed controllers (PID and NPID) based on the output response behavior and the desired performance. This section is focused on determining the optimal value of the PID and NPID controller parameters [46]- [48].

The first step is the generation of the initial population. The initial population represents zero patients. It contains three columns (K_p, K_i and K_d) for the PID controller and six columns (K_p, K_i, K_d, ω_1, ω_2 and ω_3) for the NPID controller and n rows (number of solutions). As in the COVID-19 epidemic scenario, it recognizes the first human being infected.

In the second step, the disease spread depends on the behavior of the population matrix (zero patients), several cases can be considered. The first case is some of the infected individuals die. The possibility of death is according to the COVID-19 virus death rate. Such individuals can no longer infect new individuals. The second case is the individuals surviving the COVID-19 virus will infect new individuals (intensification). Therefore, two types of disease propagation are taken into account, according to a given probability. For

ordinary spreaders, infected individuals will infect new ones according to the rate of spreading rate while if the COVID-19 virus spreading is high, the infected individuals will infect new ones according to the COVID-19 virus super spreading rate. Both ordinary and super-spreaders individuals can follow and find solutions quite dissimilarly. Therefore, individuals have a probability of traveling thus allowing them to spread the disease to solutions that may be quite different.

The third step, modernizing populations: Three populations are preserved and updated for each generation. Dead population: If any individual dies, it is added to this population and can never be used again. Recovered population: After each iteration, infected individuals (after spreading the COVID-19 virus according to the previous step) are sent to the recovered population. It is known that there is a reinfection probability. Hence, an individual fitting to this population could be re-infected at any iteration provided that it matches the reinfection criterion.

Another condition must be measured since individuals can be isolated simulating they are executing the social distancing procedures. For easiness, it is considered that an isolated individual is sent to the recovered population as well when meeting an isolation probability.

Recently, a newly infected population: This population collects all individuals infected at each iteration, according to the procedure described in the previous steps. It is possible that repeated new infected individuals are created at each iteration and, consequently,

It is recommended to eliminate such repeated individuals from this population before the next iteration starts running. The Vaccines consider the used objective function, which can treat the infected population.

The fourth step is the stop criterion. One of the most important features of the proposed algorithm lies in its capability to end without the need of controlling any parameter. This situation occurs because the recovered and dead populations are constantly increasing as time goes by, and the newly infected population cannot infect new individuals. It is estimated that the number of infected individuals increases for a certain number of iterations. However, from a particular iteration on, the size of the newly infected population will be smaller than that of the current one because recovered and dead populations are too big, and the size of the infected population decays over time.

The initial population contains the upper and lower values of the PID and NPID controller parameters for example the PID population matrix is shown in the equations from (18) to (20).

$$X = \begin{bmatrix} K_{P0} & K_{I0} & K_{D0} \\ . & . & . \\ . & . & . \\ . & . & . \\ K_{Pn} & K_{In} & K_{Dn} \end{bmatrix} \quad (18)$$

$$L_X = [K_{P0} \quad K_{I0} \quad K_{D0}] \quad (19)$$

$$U_X = [K_{Pn} \quad K_{In} \quad K_{Dn}] \quad (20)$$

The performance of each row will be investigated according to the objective function in equation (21) to (25). The poor performance specifies the infected population, which can die. While the good performance indicates the recovered population from COVID-19. The COVID-19 optimization parameters is the same as in [15].

$$K_t = (K_1 + K_2 + K_3 + K_4)/4 \quad (21)$$

$$K_1 = \frac{|t_r - t_{rd}|}{t_{rd}} \quad (22)$$

$$K_2 = \frac{|t_s - t_{sd}|}{t_{sd}} \quad (23)$$

$$K_3 = \frac{|e_{ss} - e_{ssd}|}{e_{ssd}} \quad (24)$$

$$K_4 = \frac{|OS - OS_d|}{OS_d} \quad (25)$$

where (t_{rd}) is the desired rise time and (t_r) is the measured rise time, (OS_d) is the desired maximum overshoot and (OS) is the actual overshoot, (t_{sd}) is the desired settling time and (t_s) is the determining settling time, and (e_{ssd}) is the desired steady-state error and (e_{ss}) is the estimated steady-state error.

It can be demonstrated that the objective function seeks to fulfill the designer's needs using four sub-objective functions.

The first sub-objective function emphasizes improving the rise time of overall drive systems. The second sub-objective function tries to reduce the settling time. The third sub-objective function measures the steady-state error. The fourth sub-objective function investigates the required overshoot. The value of each sub-objective function ranges from zero to one. So, the overall objective function considers the average of the sum of four sub-objective functions.

IV. Auto-Tuning Nonlinear PID Control

The Model Reference Adaptive Control (MRAC) is a high-ranking adaptive controller [49], [43], [50], [42]. It may be regarded as an adaptive servo system in which the desired performance is expressed in terms of a reference model [51]-[60]-[62]. In this work, the NPID control parameters will be adjusted online using the model reference adaptive technique and the nonlinear function. Fig. 4 presents the main structure of auto-tuning NPID based on the model reference technique.

The proposed form of NLPID control can be described as (26).

$$u(t)=(k_p + \aleph_{n1}(e))[\,e(t)]+(k_i + \aleph_{n2}(e)).\int_0^t [\,e(t)]\,dt+(k_d+\aleph_{n3}(e)).\left[\frac{de(t)}{dt}\right] \quad (26)$$

where $\aleph_{n1}(e), \aleph_{n2}(e)$ and $\aleph_{n3}(e)$ are nonlinear gains. The nonlinear gains represent any general nonlinear function of the error which is bounded in the sector $0 < \aleph_n(e) < \aleph_n(e)max$.

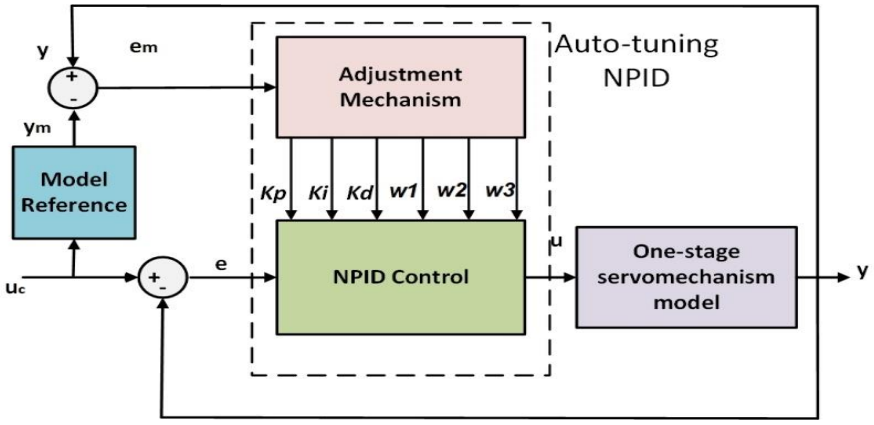

Fig. 4. The overall system with self-tuning NPID is based on model reference technique.

There is a wide range of choices available for the nonlinear gain $\aleph_n(e)$. One simple form of the nonlinear gain function can be described as (27).

$$\aleph_{nl}(e) = ch(w_i e) = \frac{exp(w_i e) + exp(-w_i e)}{2} \quad (27)$$

where $i = 1, 2, 3$.

$$e = \begin{cases} e & |e| \le e_{max} \\ e_{max} sgn(e) & |e| > e_{max} \end{cases}$$

The nonlinear gain $\aleph_n(e)$ is lower bounded by $K\_n\,(e)min = 1$ when $e = 0$, and upper-bounded by $K\_n\,(e)max = ch(w\_i\ e\_max)$. Therefore, e_{max} stand for the range of deviation, and w_i describes the rate of variation of $\aleph_n(e)$.

The MIT rule is the original approach to model reference adaptive control. The name is derived from the fact that it was developed at the Instrumentation Laboratory (now the Draper Laboratory) at MIT. To adjust parameters in such a way that the loss function is minimized as in (28).

$$j(\underline{\theta}) = \frac{1}{2} e_m^2 \quad (28)$$

To make j small, it is reasonable to change the parameters in the direction of the negative gradient of j, that is obtained as (29) and (30),

$$\frac{d\underline{\theta}}{dt} = -\gamma \frac{\partial j}{\partial \underline{\theta}} = -\gamma e_m \frac{\partial e_m}{\partial \underline{\theta}} \quad (29)$$

$$e = u_c - y \quad (30)$$

Assume that the plant can be simplified to a first order system as obvious in the equation (31).

$$\frac{y(s)}{u(s)} = \frac{k}{Ts + 1} \quad (31)$$

where k and T are unknown parameters. Also, assume that the model reference takes a form first order system as the following relationship in (32).

$$\frac{y_m(s)}{u_c(s)} = \frac{k_m}{T_m s + 1} \quad (32)$$

where k_m and T_m are selected by designer.

From equations (30) to (32) can obtained as equations (33) to (40).

$$y = \frac{k}{Ts + 1}[(k_p + \aleph_{n1}) + (k_i + \aleph_{n2})\frac{1}{s} + (k_d + \aleph_{n3})s](u_c - y) \quad (33)$$

$$y = \frac{k\left[(k_p + \aleph_{n1}) + (k_i + \aleph_{n2})\frac{1}{s} + (k_d + \aleph_{n3})s\right]}{Ts + 1} u_c - \frac{k[(k_p + \aleph_{n1}) + (k_i + \aleph_{n2})\frac{1}{s} + (k_d + \aleph_{n3})s]}{Ts + 1} y \quad (34)$$

$$\left(1 + \frac{k\left[(k_p + \aleph_{n1}) + (k_i + K_{n2})\frac{1}{s} + (k_d + \aleph_{n3})s\right]}{Ts + 1}\right) y = \frac{k[(k_p + \aleph_{n1}) + (k_i + \aleph_{n2})\frac{1}{s} + (k_d + \aleph_{n3})s]}{Ts + 1} u_c \quad (35)$$

$$\left(\frac{Ts + 1 + k\left[(k_p + \aleph_{n1}) + (k_i + \aleph_{n2})\frac{1}{s} + (k_d + \aleph_{n3})s\right]}{Ts + 1}\right) y = \frac{k[(k_p + \aleph_{n1}) + (k_i + \aleph_{n2})\frac{1}{s} + (k_d + \aleph_{n3})s]}{Ts + 1} u_c \quad (36)$$

$$y = \frac{k\left[(k_p + \aleph_{n1}) + (k_i + \aleph_{n2})\frac{1}{s} + (k_d + \aleph_{n3})s\right]}{Ts + 1 + k\left[(k_p + \aleph_{n1}) + (k_i + \aleph_{n2})\frac{1}{s} + (k_d + \aleph_{n3})s\right]} u_c \quad (37)$$

$$e_m = y - y_m \quad (38)$$

$$e_m = \left[\frac{k\left[(k_p + \aleph_{n1}) + (k_i + \aleph_{n2})\frac{1}{s} + (k_d + K_{n3})s\right]}{Ts + 1 + k\left[(k_p + \aleph_{n1}) + (k_i + \aleph_{n2})\frac{1}{s} + (k_d + \aleph_{n3})s\right]} - \frac{k_m}{T_m s + 1}\right] u_c \quad (39)$$

$$\frac{\partial e_m}{\partial k_p} = \left[\frac{(Ts+1)k}{\left(Ts + k[(k_p + \aleph_{n1}) + (k_i + \aleph_{n2})\frac{1}{s} + (k_d + \aleph_{n3})s]\right)^2}\right]u_c \quad (40)$$

Equation (24) can be rewritten be (41).

$$\frac{\partial e_m}{\partial k_p} = \left[\frac{(Ts+1)k}{\left(Ts + k\left[(k_p + \aleph_{n1}) + (k_i + \aleph_{n2})\frac{1}{s} + (k_d + \aleph_{n3})s\right] + 1\right)} \quad (41)$$

$$\frac{}{\left(k\left[(k_p + \aleph_{n1}) + (k_i + \aleph_{n2})\frac{1}{s} + (k_d + \aleph_{n3})s\right]\right)}\Bigg]y$$

From equation (27) and equation (33), obtained new model as in (42).

$$\frac{\partial e_m}{\partial k_p} = \left[\frac{k^2 e}{\left(Ts + k[(k_p + \aleph_{n1}) + (k_i + \aleph_{n2})\frac{1}{s} + (k_d + \aleph_{n3})s] + 1\right)}\right] \quad (42)$$

To achieve the desired performance, the following condition must be hold as in (43) and (44).

$$Ts + k[(k_p + \aleph_{n1}) + (k_i + \aleph_{n2})\frac{1}{s} + (k_d + \aleph_{n3})s] + 1 = T_m s + 1 \quad (43)$$

$$\frac{\partial e_m}{\partial k_p} = \frac{k^2 e}{T_m s + 1} \quad (44)$$

From the MIT rule can obtain as equations (45) to (48) for the following relationship

$$\frac{dk_p}{dt} = -\gamma . e_m . \frac{k^2 e}{T_m s + 1} \quad (45)$$

$$\frac{dk_p}{dt} = -\gamma_1 . \frac{e_m . e}{T_m s + 1} \quad (46)$$

$$\gamma_1 = \gamma . k^2 \quad (47)$$

$$k_p)_{new} = \int \frac{dk_p}{dt}\, dt + k_p(0) \quad (48)$$

where $k_p(0)$ is the initial value of proportional gain k_p obtained as (49).

$$\frac{\partial e_m}{\partial k_i} = \frac{1}{s}\left[\frac{k}{Ts + k\left[(k_p + \aleph_{n1}) + (k_i + \aleph_{n2})\frac{1}{s} + (k_d + \aleph_{n3})s\right] + 1} \right. \quad (49)$$

$$\left. - \frac{k[(k_p + \aleph_{n1}) + (k_i + \aleph_{n2})\frac{1}{s} + (k_d + \aleph_{n3})s]}{\left(Ts + k[(k_p + \aleph_{n1}) + (k_i + \aleph_{n2})\frac{1}{s} + (k_d + \aleph_{n3})s] + 1\right)^2}\right]u_c$$

Equation (45) can be rewritten to be (50) and (51).

$$\frac{\partial e_m}{\partial k_i} = \frac{1}{s}\left[\frac{k(Ts+1)}{\left(Ts + k\left[(k_p + \aleph_{n1}) + (k_i + \aleph_{n2})\frac{1}{s} + (k_d + \aleph_{n3})s\right] + 1\right)^2}\right] \quad (50)$$

$$\frac{\partial e_m}{\partial k_i} = \frac{1}{s}\left[\frac{k(Ts+1)}{\left(Ts + k\left[(k_p + \aleph_{n1}) + (k_i + \aleph_{n2})\frac{1}{s} + (k_d + \aleph_{n3})s\right] + 1\right)} \quad (51)$$

$$\frac{}{\left(k\left[(k_p + \aleph_{n1}) + (k_i + \aleph_{n2})\frac{1}{s} + (k_d + \aleph_{n3})s\right]\right)}\Bigg]y$$

From equation (49) and equation (51) obtained model as in (52).

$$\frac{\partial e_m}{\partial k_i} = \frac{1}{s}\left[\frac{k^2 e}{\left(Ts + k[(k_p + \aleph_{n1}) + (k_i + \aleph_{n2})\frac{1}{s} + (k_d + \aleph_{n3})s] + 1\right)}\right] \quad (52)$$

To achieve the desired performance, the condition must be hold in equation (53).

$$\frac{\partial e_m}{\partial k_i} = \frac{1}{s}\frac{k^2 e}{T_m s + 1} \quad (53)$$

From the MIT rule can obtain equations (54) to (57) for the following relationship.

$$\frac{dk_i}{dt} = -\gamma . e_m . \frac{1}{s}\frac{k^2 e}{T_m s + 1} \quad (54)$$

$$\frac{dk_i}{dt} = -\gamma_2 . \frac{e_m . e}{T_m s + 1} \quad (55)$$

$$\gamma_2 = \gamma k^2 . \frac{1}{s} = \gamma_1 \frac{1}{s} \quad (56)$$

$$k_i)_{new} = \int \frac{dk_i}{dt}\, dt + k_i(0) \quad (57)$$

where $k_i(0)$ is the initial value of proportional gain k_i obtained as equations (58) to (61).

$$\frac{\partial e_m}{\partial k_d} = \left[\frac{ks}{Ts + k\left[(k_p + \aleph_{n1}) + (k_i + \aleph_{n2})\frac{1}{s} + (k_d + \aleph_{n3})s\right] + 1} \right. \quad (58)$$

$$\left. - \frac{ks\left(k[(k_p + \aleph_{n1}) + (k_i + \aleph_{n2})\frac{1}{s} + (k_d + \aleph_{n3})s]\right)}{\left(Ts + k[(k_p + \aleph_{n1}) + (k_i + \aleph_{n2})\frac{1}{s} + (k_d + \aleph_{n3})s] + 1\right)^2}\right]u_c$$

$$\frac{\partial e_m}{\partial k_d} = \left[\frac{ks^{\mu}\left(Ts + k\left[(k_p + \aleph_{n1}) + (k_i + \aleph_{n2})\frac{1}{s} + (k_d + \aleph_{n3})s\right]\right.}{\left(Ts + k\left[(k_p + \aleph_{n1}) + (k_i + \aleph_{n2})\frac{1}{s}\right.\right.} \quad (59)$$

$$\left.\frac{+1-k[(k_p+\aleph_{n1})+(k_i+\aleph_{n2})\frac{1}{s}+(k_d+\aleph_{n3})s])}{+(k_d+\aleph_{n3})s]+1)^2}\right]u_c$$

$$\frac{\partial e_m}{\partial k_d}=\left[\frac{ks(Ts+1)}{\left(Ts+k\left[[(k_p+\aleph_{n1})+(k_i+\aleph_{n2})\frac{1}{s}+(k_d+\aleph_{n3})s\right]+1\right)^2}\right]u_c \quad (60)$$

$$\frac{\partial e_m}{\partial k_d}=\left[\frac{ks(Ts+1)}{\left(Ts+k\left[(k_p+\aleph_{n1})+(k_i+K_{n2})\frac{1}{s}+(k_d+\aleph_{n3})s\right]+1\right)}\right.$$
$$\left.\frac{}{\left(k\left[(k_p+\aleph_{n1})+(k_i+\aleph_{n2})\frac{1}{s}+(k_d+\aleph_{n3})s\right]\right)}\right]y \quad (61)$$

Also, from equation (59) and equation (61), can be obtained as equations (62) to (67).

$$\frac{\partial e_m}{\partial k_d}=\left[\frac{k^2.s.e}{\left(Ts+k[(k_p+\aleph_{n1})+(k_i+\aleph_{n2})\frac{1}{s}+(k_d+\aleph_{n3})s]+1\right)}\right] \quad (62)$$

$$\frac{\partial e_m}{\partial k_d}=\frac{k^2.s.e}{T_m s+1} \quad (63)$$

$$\frac{dk_d}{dt}=-\gamma.e_m.\frac{k^2.s.e}{T_m s+1} \quad (64)$$

$$\frac{dk_d}{dt}=-\gamma_3.\frac{e_m.e}{T_m s+1} \quad (65)$$

$$\gamma_3=\gamma.k^2.s=\gamma_1.s \quad (66)$$

$$k_d)_{new}=\int\frac{dk_d}{dt}\,dt+k_d(0) \quad (67)$$

where $k_d(0)$ is the initial value of derivative gain k_d.

V. RESULTS AND DISCUSSION

This section demonstrates the motion control behavior of the one axis servomechanism using several control techniques. Two models of servomechanism were developed, the first is the model without uncertainty and the second is the model with parameter uncertainty. The PID control technique was applied on the two models to investigate the system performance. The other control techniques. The other control techniques used the model with uncertainty and nonlinear behavior. Two tests had been implemented, the first measures the motion accuracy through a step operating point. The second investigates the performance through a stair operating points.

Fig. 5 demonstrates the PID closed loop dynamic behavior of the servomechanism through a single operating speed. It can be noted that the difference between the output of linear and nonlinear models. The stage reaches the operating point through a 5 seconds which considers not satisfied for high performance applications. In case of the model with uncertainty the PID control cannot absorb the uncertainty and has a high fluctuation about the operating point. Also, the high rise time makes the performance of the system is poor and not acceptable for high accuracy industrial applications.

Fig. 6 demonstrates the corresponding controller output of the PID control for both models. It can obvious that the output of the PID control suffers from high shuttering due to the system uncertainty. Also, it try to realize the reference operating point as possible. So, the other control techniques will be used to treat this problem.

Fig. 7 illustrates a comparative study between the PID control, NPID control and the self-tuning NPID control for test one (step operating point). It can be noted that the self-tuning NPID control has a low rise time among other techniques. Also, the proposed self-tuning NPID control not has a fluctuations about the reference operating point. The NPID control suffers from a high overshoot and high fluctuations about the reference point.

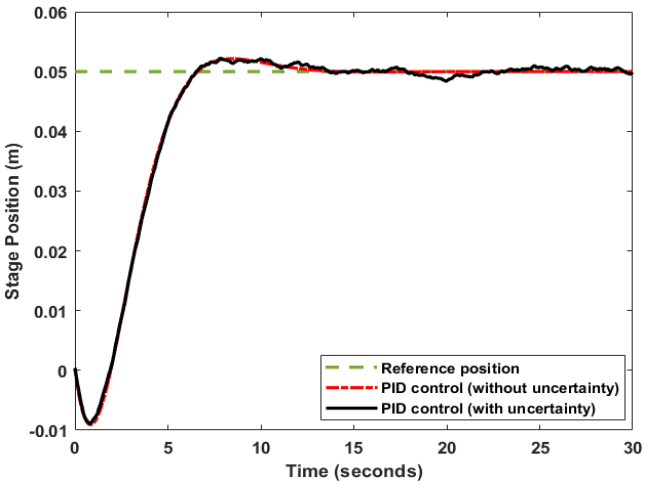

Fig. 5. The stage position response at step reference using the PID control.

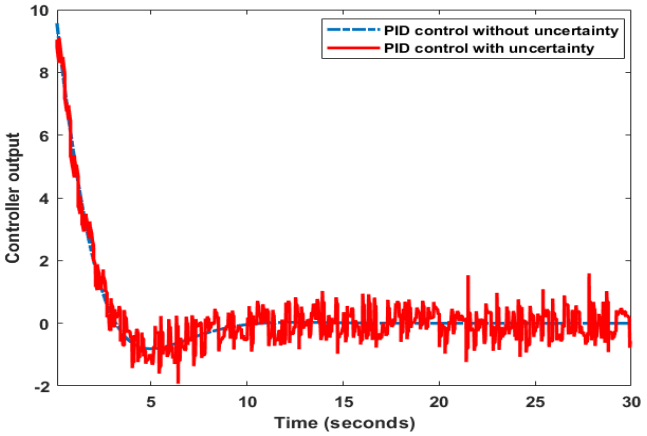

Fig. 6. The corresponding PID controller output the motor through a fixed speed reference.

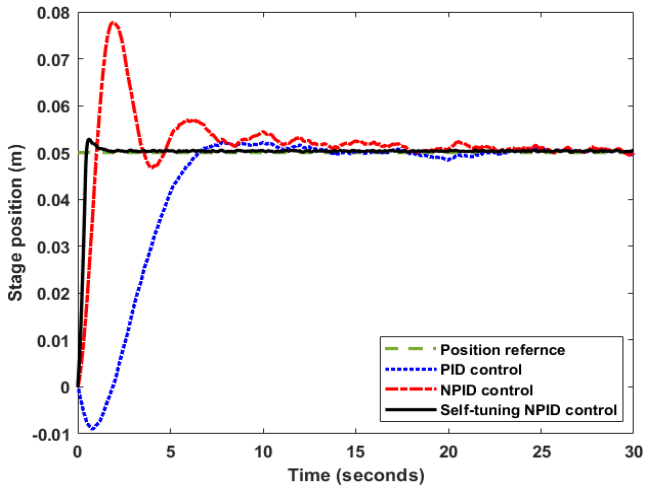

Fig. 7. Performance of the PID, NPID, and self-tuning NPID to track a step reference position test.

Fig. 8 demonstrates the corresponding controller output. It is demonstrated that the PID and self-tuning NPID controller have a high starting value. In contrast, the NPID has a low starting output. Also, it is noted that the PID output has a high shuttering compared to other control techniques.

Fig. 9 shows the performance of the control techniques for the second test (stair operating point). It is illustrated that the self-tuning NPID control has a high accuracy in tracking and following the continuous change of the operating point. In case of the PID and NPID controllers, they suffer from a high delay compared to the self-tuning NPID control.

Fig. 10 display the corresponding controller output for continuous change of operating point test. It is illustrated that the self-tuning NPID controller has a high starting value at each new operating point. Also, the change in controller output is faster than the PID and NPID controllers which makes the self-tuning NPID tack accurately the position reference and absorb the system uncertainty.

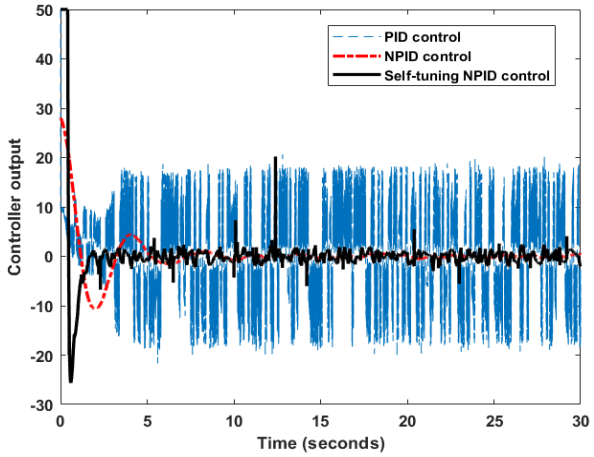

Fig. 8. The corresponding output of the PID, NPID, and self-tuning NPID to track a step reference position test.

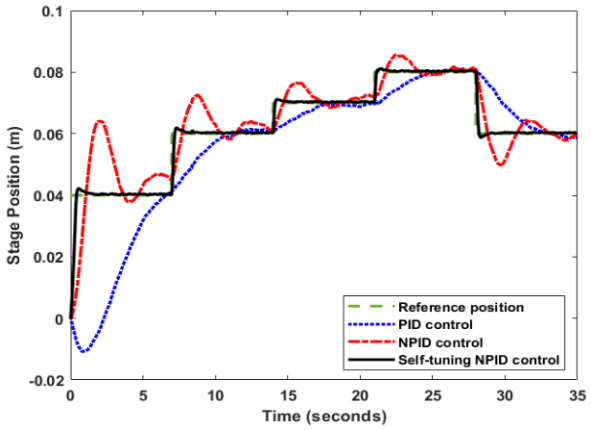

Fig. 9. The system motion behavior for the PID, NPID, and self-tuning NPID to track a continuous reference position test

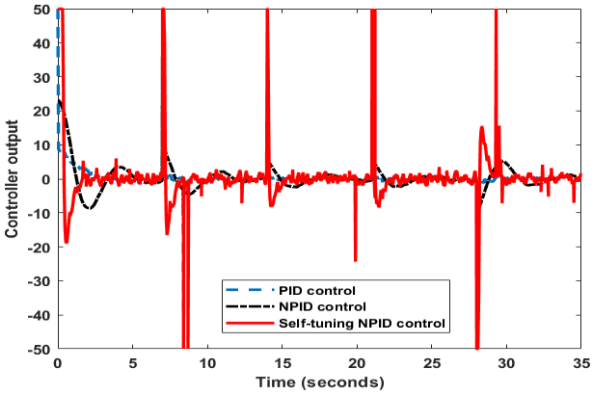

Fig. 10. The corresponding output of the PID, NPID, and self-tuning NPID to track a step reference position test.

VI. Conclusion

In this research, a novel one-axis servomechanism investigation is presented, taking into account parameter fluctuation and system uncertainty. Additionally, a novel method for very effective self-tuning nonlinear PID control was created to accurately monitor a chosen profile. A comparative study between the suggested control method and the well-known controllers is also included (PID and Nonlinear PID). The COVID-19 optimization technique was used to determine the best control parameters. Through the online simulation, the servomechanism system's settings were modified at random within a predetermined range. As nonlinearity resources (friction, backlash, environmental influences), these parameters fluctuate and contribute to system uncertainty. It had been completed and looked at to compare the linear and nonlinear models. The findings demonstrate that the suggested controller has a high tracking accuracy, a rapid rise time, and a low overshoot.

References

[1] M. Marsono, Y. Yoto, A. Suyetno, and R. Nurmalasari, "Design and programming of 5 axis manipulator robot with grblgru open source software on preparing vocational students' robotic skills," *Journal of Robotics and Control*, vol. 2, no. 6, pp. 539–545, 2021.

[2] F. N. Abdullah, G. A. Aziz, and S. W. Shneen, "Simulation Model of Servo Motor by Using Matlab," *Journal of Robotics and Control*, vol. 3, no. 2, pp. 176–179, 2022.

[3] F. B. Setiawan, P. M. Siva, L. H. Pratomo, and S. Riyadi, "Design and implementation of smart forklift for automatic guided vehicle using

raspberry pi 4," *Journal of Robotics and Control*, vol. 2, no. 6, pp. 508–514, 2021.

[4] M. Saad, A. H. Amhedb, and M. Al Sharqawi, "Real time DC motor position control using PID controller in LabVIEW," *Journal of Robotics and Control*, vol. 2, no. 5, pp. 342–348, 2021.

[5] M. Abdullah-Al-Noman, A. N. Eva, T. B. Yeahyea, and R. Khan, "Computer Vision-based Robotic Arm for Object Color, Shape, and Size Detection," *Journal of Robotics and Control*, vol. 3, no. 2, pp. 180–186, 2022.

[6] M. R. Islam1, M. R. T. Hossain2, and S. C. Banik, "Synchronizing of stabilizing platform mounted on a two-wheeled robot," *Journal of Robotics and Control*, vol. 2, no. 6, pp. 552–558, 2021.

[7] Khairunisa, Mardeni, and Y. Irawan, "Smart aquarium design using raspberry Pi and android based," *Journal of Robotics and Control*, vol. 2, no. 5, pp. 368–372, 2021.

[8] D. M. Harfina, Z. Zaini, and W. J. Wulung, "Disinfectant spraying system with quadcopter type unmanned aerial vehicle technology as an effort to break the chain of the covid-19 virus," *Journal of Robotics and Control*, vol. 2, no. 6, pp. 502–507, 2021.

[9] H. Maghfiroh, M. Ahmad, A. Ramelan, and F. Adriyanto, "Fuzzy-PID in BLDC Motor Speed Control Using MATLAB/Simulink," *Journal of Robotics and Control*, vol. 3, no. 1, pp. 8–13, 2022.

[10] I. Suwarno, Y. Finayani, R. Rahim, J. Alhamid, and A. R. Al-Obaidi, "Controllability and Observability Analysis of DC Motor System and a Design of FLC-Based Speed Control Algorithm," *Journal of Robotics and Control*, vol. 3, no. 2, pp. 227–235, 2022.

[11] A. Ma'arif and A. Çakan, "Simulation and arduino hardware implementation of dc motor control using sliding mode controller," *Journal of Robotics and Control*, vol. 2, no. 6, pp. 582–587, 2021.

[12] S. R. Utama, A. Firdausi, and G. P. N. Hakim, "Control and Monitoring Automatic Floodgate Based on NodeMCU and IOT with Fuzzy Logic Testing," *Journal of Robotics and Control*, vol. 3, no. 1, pp. 14–17, 2022.

[13] M. A. Mossa, H. Khouidmi, and A. Ma'arif, "Robust Flux and Speed State Observer Design for Sensorless Control of a Double Star Induction Motor," *Journal of Robotics and Control*, vol. 3, no. 4, pp. 464–475, 2022.

[14] Y. Zahraoui, M. Akherraz, C. Fahassa, and S. Elbadaoui, "Induction Motor DTC Performance Improvement by Reducing Flux and Torque Ripples in Low Speed," *Journal of Robotics and Control*, vol. 3, no. 1, pp. 93–100, 2022.

[15] M. A. Shamseldin, "Optimal Covid-19 Based PD/PID Cascaded Tracking Control for Robot Arm driven by BLDC Motor," *WSEAS Transactions on Systems*, vol. 20, pp. 217–227, 2021.

[16] N. P. Van Bach, Q. D. Hai, and T. B. Trung, "Optimization of trajectory tracking control of 3-DOF translational robot use PSO method based on inverse dynamics control for surgery application," *Journal of Vibroengineering*, vol. 23, no. 7, pp. 1591-1601, 2021.

[17] Y. Zahraoui, M. Moutchou, S. Tayane, C. Fahassa, S. Elbadaoui, and A. Ma'arif, "Synchronous Reluctance Motor Performance Improvement Using MTPA Control Strategy and Five-Level Inverter Topology," *Journal of Robotics and Control (JRC)*, vol. 3, no. 5, pp. 725-734, 2022.

[18] R. M. Sari, E. Sabna, R. Wahyuni, and Y. Irawan, "Implementation of open and close a housing gate portal using RFID card," *Journal of Robotics and Control*, vol. 2, no. 5, pp. 363–367, 2021.

[19] A. L. Shuraiji and S. W. Shneen, "Fuzzy Logic Control and PID Controller for Brushless Permanent Magnetic Direct Current Motor: A Comparative Study," *Journal of Robotics and Control*, vol. 3, no. 6, pp. 762–768, 2022.

[20] A. Latif, A. Z. Arfianto, H. A. Widodo, R. Rahim, and E. T. Helmy, "Motor DC PID system regulator for mini conveyor drive based-on matlab," *Journal of Robotics and Control*, vol. 1, no. 6, pp. 185–190, 2020.

[21] A. Ma'arif and N. R. Setiawan, "Control of dc motor using integral state feedback and comparison with pid: Simulation and arduino implementation," *Journal of Robotics and Control*, vol. 2, no. 5, pp. 456–461, 2021.

[22] K. Kunal, A. Z. Arfianto, J. E. Poetro, F. Waseel, and R. A. Atmoko, "Accelerometer implementation as feedback on 5 degree of freedom arm robot," *Journal of Robotics and Control*, vol. 1, no. 1, pp. 31–34, 2020.

[23] Y. Irawan, Muhardi, R. Ordila, and R. Diandra, "Automatic floor cleaning robot using arduino and ultrasonic sensor," *Journal of Robotics and Control*, vol. 2, no. 4, pp. 240–243, 2021.

[24] A. A. Rafiq, W. N. Rohman, and S. D. Riyanto, "Development of a simple and low-cost smartphone gimbal with MPU-6050 sensor," *Journal of Robotics and Control*, vol. 1, no. 4, pp. 136–140, 2020.

[25] A. W. L. Yao and H. C. Chen, "An Intelligent Color Image Recognition and Mobile Control System for Robotic Arm," *International Journal of Robotics and Control Systems*, vol. 2, no. 1, pp. 97–104, 2022.

[26] Y. Irawan, R. Wahyuni, and H. Fonda, "Folding clothes tool using arduino uno microcontroller and gear servo," *Journal of Robotics and Control*, vol. 2, no. 3, pp. 170–174, 2021.

[27] D. Handaya and R. Fauziah, "Proportional-integral-derivative and linear quadratic regulator control of direct current motor position using multi-turn based on LabView," *Journal of Robotics and Control*, vol. 2, no. 4, pp. 332–336, 2021.

[28] N. S. Shalal and W. S. Aboud, "Smart robotic exoskeleton: A 3-dof for wrist-forearm rehabilitation," *Journal of Robotics and Control*, vol. 2, no. 6, pp. 476–483, 2021.

[29] R. R. Ardeshiri, H. N. Kashani, and A. Reza-Ahrabi, "Design and simulation of self-Tuning fractional order fuzzy PID controller for robotic manipulator," *International Journal of Automation and Control*, vol. 13, no. 5, pp. 595–618, 2019.

[30] R. ÇELİKEL, "Speed Control of BLDC Using NARMA-L2 Controller in Single Link Manipulator," *Balkan Journal of Electrical and Computer Engineering*, vol. 7, no. 2, 2019.

[31] C. Systems and C. S. Engineering, "Optimal Feedback Compensator Design Tuned with GA for Adaptive Controllers with Experimental Application for Brushless DC Motor," 2020.

[32] M. A. Eissa, A. Sali, F. A. Ahmad, and R. R. Darwish, "Observer-Based Fault Detection Approach Using Fuzzy Adaptive Poles Placement System with Real-Time Implementation," *IEEE Access*, vol. 9, pp. 83272–83284, 2021.

[33] M. A. Eissa, A. Sali, M. K. Hassan, A. M. Bassiuny, and R. R. Darwish, "Observer-Based Fault Detection with Fuzzy Variable Gains and Its Application to Industrial Servo System," *IEEE Access*, vol. 8, pp. 131224–131238, 2020.

[34] H. Chhabra, V. Mohan, A. Rani, and V. Singh, "Robust nonlinear fractional order fuzzy PD plus fuzzy I controller applied to robotic manipulator," *Neural Comput. Appl.*, vol. 32, no. 7, pp. 2055–2079, 2020.

[35] B. Zhang, G. Cheng and J. -g. Hu, "An expanded proximate time-optimal servo controller design for fast set-point motion," *2016 35th Chinese Control Conference (CCC)*, pp. 4465-4470, 2016.

[36] C. Abeykoon, "Single screw extrusion control: A comprehensive review and directions for improvements," *Control Engineering Practice*, vol. 51, pp. 69–80, 2016.

[37] P. Zhao and Y. Shi, "Robust control of the A-axis with friction variation and parameters uncertainty in five-axis CNC machine tools," *Proceedings of the Institution of Mechanical Engineers, Part C: Journal of Mechanical Engineering Science*, vol. 228, no. 14, pp. 2545–2556, 2014.

[38] F. T. Li, L. Ma, L. T. Mi, Y. X. Zeng, N. B. Jin, and Y. L. Gao, "Friction identification and compensation design for precision positioning," *Advances in Manufacturing*, vol. 5, no. 2, pp. 120–129, 2017.

[39] M. Omar, M. A. Ebrahim, A. M. AbdelGhany, and F. Bendary, "Tuning of PID controller for load frequency control problem via harmony search algorithm," *Indonesian Journal of Electrical Engineering and Computer Science*, vol. 1, no. 2, pp. 255–263, 2016.

[40] L. M. El-Tehewy, M. A. Shamseldin, M. Sallam, and A. A. Ghany, "A Modified Model Reference Adaptive Control for High-Performance Pantograph Robot Mechanism," *WSEAS Transactions on Applied and Theoretical Mechanics*, vol. 16, pp. 193-203, 2021.

[41] B. Feng, D. Zhang, J. Yang, and S. Guo, "A novel time-varying friction compensation method for servomechanism," *Mathematical Problems in Engineering*, vol. 2015, 2015.

[42] C. Wang, M. Yang, W. Zheng, X. Lv, K. Hu, and D. Xu, "Analysis of limit cycle mechanism for two-mass system with backlash

nonlinearity," *IECON 2016 - 42nd Annual Conference of the IEEE Industrial Electronics Society*, pp. 500–505, 2016.

[43] M. Chang and G. Guo, "Sinusoidal Servocompensator Implementations with Real-Time Requirements and Applications," *IEEE Transactions on Control Systems Technology*, vol. 25, no. 2, pp. 645–652, 2017.

[44] F. Wang, C. Liang, Z. Ma, X. Zhao, Y. Tian, and D. Zhang, "Dynamic analysis of an XY positioning table," *2013 International Conference on Manipulation, Manufacturing and Measurement on the Nanoscale*, pp. 211–214, 2013.

[45] L. Abdullah *et al*., "Evaluation on tracking performance of PID, gain scheduling and classical cascade P/PI controller on XY table ballscrew drive system," *World Applied Sciences Journal*, vol. 21, no. special issue, pp. 1–10, 2013.

[46] K. Kozioł, R. Stanisławski, and G. Bialic, "Fractional-order sir epidemic model for transmission prediction of COVID-19 disease," *Applied Sciences*, vol. 10, no. 23, pp. 1–9, 2020.

[47] M. A. Shamseldin, "Optimal Coronavirus Optimization Algorithm Based PID Controller for High Performance Brushless DC Motor," *Algorithms*, vol. 14, no. 7, p. 193, 2021.

[48] F. Martínez-Álvarez *et al*., "Coronavirus Optimization Algorithm: A Bioinspired Metaheuristic Based on the COVID-19 Propagation Model," *Big Data*, vol. 8, no. 4, pp. 308–322, 2020.

[49] E. Yuliza, H. Habil, R. A. Salam, M. M. Munir, M. Abdullah, and Khairurrijal, "Development of a Simple Single-Axis Motion Table System for Testing Tilt Sensors," *Procedia Engineering*, vol. 170, pp. 378–383, 2017.

[50] J. Heidenhain, "Dynamic Precision – Machining Dynamically and with High Accuracy Dynamic Precision Shorter machining times, higher accuracy, better surfaces," 2013.

[51] B. A. Saputra, E. P. Hidayat, and A. Z. Arfianto, "Internet of things-based steam pump motor protection due to voltage unbalance," *Journal of Robotics and Control (JRC)*, vol. 1, no. 2, pp. 64–69, 2020.

[52] P. Perz, I. Malujda, D. Wilczyński, and P. Tarkowski, "Methods of Controlling a Hybrid Positioning System Using LabVIEW," Procedia Engineering, vol. 177, pp. 339–346, 2017.

[53] A. Iftar, "Robust servomechanism problem for robotic systems described by delay-differential-algebraic equations," *2015 IEEE 7th International Conference on Cybernetics and Intelligent Systems (CIS) and IEEE Conference on Robotics, Automation and Mechatronics (RAM)*, vol. 2, no. 1, pp. 13–18, 2015.

[54] E. Cajueiro, R. Kalid, and L. Schnitman, "Using NARX model with wavelet network to inferring the polished rod position," *International journal of Mathematics and Computers in simulation*, vol. 6, no. 1, pp. 66–73, 2012.

[55] W. Lee, C. Y. Lee, Y. H. Jeong, and B. K. Min, "Friction compensation controller for load varying machine tool feed drive," *International Journal of Machine Tools and Manufacture*, vol. 96, pp. 47–54, 2015.

[56] R. Madiouni, "Robust PID controller design based on multi-objective Particle Swarm Optimization approach," *2017 International Conference on Engineering & MIS (ICEMIS)*, pp. 1–7, 2018.

[57] M. A. George, D. V. Kamat, and C. P. Kurian, "Electronically Tunable ACO Based Fuzzy FOPID Controller for Effective Speed Control of Electric Vehicle," *IEEE Access*, vol. 9, pp. 73392–73412, 2021.

[58] A. O. Kıyaklı and H. Solmaz, "Modeling of an Electric Vehicle with MATLAB/Simulink," *International Journal of Automotive Science and Technology*, vol. 2, no. 4, pp. 9–15, 2019.

[59] T. K.-E. Yurdaer, "Comparison of Energy Consumption of Different Electric Vehicle Power Systems Using Fuzzy Logic-Based Regenerative Braking," *Eng. Perspect.*, vol. 1, no. 1, pp. 11–21, 2021.

[60] S. S. Yeh and J. T. Sun, "Feedforward motion control design for improving contouring accuracy of CNC machine tools," *Proceedings of the International MultiConference of Engineers and Computer Scientists*, vol. 2202, pp. 111–116, 2013.

[61] H. Abdelfattah, S. A. Kotb, M. Esmail, and M. I. Mosaad, "Adaptive Neuro-Fuzzy Self-Tuned-PID Controller for," *International Journal of Robotics and Control Systems*, vol. 3, no. 1, pp. 1–18, 2023.

[62] J. Laarni, T. Tommila, and P. Savioja, "Concept of operations as a boundary object in design and knowledge sharing in nuclear industry," *International Journal of Robotics and Control Systems*, vol. 2, no. 4, pp. 692–708, 2022.